Pressure Dependent Mechanical Properties of Thin Films under Uniaxial Strain via the Layer Compression Test

Aaron D. Sinnott[1], Adam Kelly[1], Cian Gabbett[1], Matthias Mobius[1], Jonathan Coleman[1], Graham L.W. Cross[1]

1: Trinity College Dublin

Abstract

Amorphous materials can exhibit strong nonlinear mechanical properties in comparison to crystalline metals and ceramics, largely due to their non equilibrium state which depends on the means of sample preparation history. For example, glassy polymer structure is highly dependent on the speed of quenching through the glass transition which determines the degree of free volume within the system. Porous materials and composites often exhibit similar void space dependencies on preparation, for example with extrusion or spraying parameters. This can lead to variations in mechanical response of a material with strain, as the material density will change due to the alteration of free volume.

While this remains challenging to quantifying comprehensively in bulk materials, it remains almost completely unaddressed in the case of thin films where current mechanical testing techniques struggle to apply and monitor well characterised application of stress and strain required to adequately probe such effects. Given the central importance of thin film materials across many modern technologies, ranging from semiconductors to medical devices and sensors, there exists a need to adequately monitor and describe changes in amorphous thin film properties under a changing mechanical state.

In this work we present the effect of elasticity and yield pressure dependence during aligned flat punch nanoindentation of amorphous thin films in the layer compression test. Supported by finite element simulations of a pressure dependent material, we show continuous in-situ stiffening of polystyrene and sprayed graphene nanosheet networks films throughout uniaxial strain compression. We also demonstrate yielding of thin film PMMA in this geometry through the injection of additional shear

within the layer compression test, which may allow exploration of yield in thin films of materials with highly pressure sensitive yield surfaces.

Intro

Characterising the mechanisms involved in plastic deformation of glassy and amorphous solids is an ongoing and in many ways poorly understood field of materials research. While it is clear there exists a distinct yield transition from elastic to plastic deformations, the carriers of plastic deformation remain unclear. Several models have attempted to tackle the existence of plasticity carriers, including the shear transformation model which postulates that plasticity carriers do not exist before applied stress and nucleate when stress is applied, and the shear transformation zone model which puts forward that plasticity nucleates around pre-existing regions of increased structural disorder[1-5]. While there remains many unanswered questions on this topic, it is known that shear stress plays the central role in the yielding process. In particular, octahedral shear stress τ_{oct} acts to mediate material yield, as hydrostatic stress alone does not cause yielding in materials with close packed, homogeneous internal structure. This is less clear for amorphous materials, with some theories suggesting that shear may evolve around sites of disorder within the structure and allow for yielding under hydrostatic pressure[6]. In all cases though it is accepted that shear plays a fundamental role in material yield and is suppressed to varying degrees under hydrostatic stress conditions.

A material will yield when the octahedral shear stress reaches a critical value, τ_{oct_0}, related to the axial yield strength σ_0 as follows[7]:

$$\tau_{oct_0} = \frac{\sqrt{2}}{3}\sigma_0 \tag{1}$$

In the case of uniaxial strain, where axial stress is applied to a material confined in all other principal directions, the relationship between this octahedral shear stress and pressure follows from the Von Mises stress relation for uniaxial strain and is expressed as follows[6, 8]:

$$\tau_{oct} = \frac{2\sqrt{2}}{3}\frac{G}{K}P \quad (2)$$

Where *P* is the applied pressure, *G* is the shear modulus, and *K* is the bulk modulus. As pressure increases, so too will the octahedral shear stress, and when this becomes greater than the required τ_{oct_0}, the material will yield. However, for amorphous materials it is known that the required τ_{oct} for yield can also increase with applied pressure, resulting in a pressure dependant yield surface instead of a constant criterion. This pressure dependence is a linear relationship at low enough contact pressures, being, in the Von Mises condition[9, 10]:

$$\tau_{oct} = \tau_{oct_0} + \mu_{vm}P \quad (3)$$

Where μ_{vm} is the Von Mises pressure coefficient. More complex yield surfaces have been suggested for materials of various morphology. For example the well-studied Cam-clay model for soils which considers the granular nature of rough frictional particles, giving an elliptical yield surface[11, 12]. In this work we consider this more generalised Von Mises shear surface criterion.

In general, during the continued application of axial stress, the octahedral sheer stress will overtake the pressure dependant yield surface and result in a transitory yielding condition characterising a traditional elastic-plastic transition, but it is possible for the yield surface to increase faster than the octahedral yield stress and therefore for yield to never occur within approachable pressure ranges, ie the criteria of $\mu_{vm} > \frac{2\sqrt{2}}{3}\frac{G}{K}$. This condition is more common in uniaxial strain geometries which minimise shear deformations, as can be seen with experiments by Ravi-Chandar by which they found they could not cause a sample of PMMA to yield in a uniaxial strain setup[13]. Pressure dependent effects in polymers offer an insight into the propagation of strain within the material and can help enlighten the search for the carriers of plasticity in these systems. For example, the pressure dependence of the yield surface discussed earlier is generally attributed to a reduction of molecular motion at higher pressures, and the suppression of the α and β relaxations in the polymer motion[14, 15]. While these pressure effects have been known about for some time in a range of materials[16-

19], pressure dependence in polymers in general remains an important tool for understanding polymer mechanics, and an area of key consideration for mechanical testing of such systems.

More recently, thin film materials have developed as an area of large technological and scientific interest. However, mechanical testing of such supported films remains in its infancy as typical nanoindentation techniques struggle to account for the proximity of the substrate. The layer compression test (LCT) is an aligned flat punch indentation technique that shows promise as a means of extensive mechanical analysis of such supported thin films[20, 21]. Fundamental to the LCT is the approximation of a compressive uniaxial strain state on the sample of interest through combined high contact aspect ratio and confinement effects of the indenter, substrate, and surrounding film jacket. This makes it a powerful tool for probing the mechanical nature of thin films, as well as for explorations of pressure dependent effects within these systems. Fig. 1(c) shows LCT indentations on a 270 nm thick film of PMMA supported on a Si substrate with a 2μm diameter flat punch tip. Shown are indents to various maximum loads, with a clear slope transition around 0.1 strain which we attribute to a yielding event, in contrast to Ravi-Chandars observation of a lack of compressive yield in confined uniaxially compressed PMMA. In this work we explore pressure dependent effects of thin film amorphous materials. We present Finite Element (FEA) simulations of a simulated polymer in a uniaxial strain system, analysing the resulting pressure dependant yield surface behaviour. Using this we examine observed pressure dependency in compressive uniaxial strain of amorphous films using the LCT. This includes observations of pressure dependent stiffness of thin films of both polystyrene (PS) and sprayed graphene nanosheet films, as well as the features of the LCT that can facilitate yield in materials that otherwise exhibit $\mu_{vm} > \frac{2\sqrt{2}}{3}\frac{G}{K}$ such as in PMMA.

FEA Simulated Amorphous Solid Uniaxial Strain

In order to explore the pressure dependant yield surface, finite element simulations of a pressure dependant material in a confined uniaxial strain compressive geometry were performed using the

Abaqus 2019 implicit solver. Simulating the pressure dependent nature of the material was done conveniently by adapting a porous material model for elasticity with pressure dependent elastic parameters adapted from Hughes and Kelly work on second order elastic deformation[22], and a model of soft rock plasticity for yield and plastic hardening behaviour beyond the yield point[23, 24]. Porous elasticity was chosen due to the fundamental nature of polymer glass morphology, whereby in finite quenching times the monomer chains settle into a glassy solid state in a nonequilibrium configuration. This nonequilibrium state is characterised by large areas of free-volume, which may be reduced by thermal annealing and long quenching times, or by compression of the material[14]. As such, the elastic behaviour of the solid can be modelled as a porous system, where the reduction of free volume within the system leads to a change in mechanical characteristics via limitation of polymer chain and sidegroup motion. For this we use a reference Young's modulus of 4.8 GPa, a variable Poisson's ratio of ν_0 = 0.34 at zero pressure and ν = 0.395 at infinite pressure. The initial pressure stress p_0 was set to 0.67 GPa where $p_0 = -\frac{1}{3}\left(\sigma_{11_0} + \sigma_{22_0} + \sigma_{33_0}\right)$

For the plastic portion, the variable pressure dependant yield surface feature of the built in Abaqus soft rock plasticity model was exploited, while all other effects like strain hardening were turned off. The compressive yield stress was set to 20 GPa, and the tensile yield stress to 0.53 GPa. The yield surface in this model is defined by the angle ψ, which is the friction angle, or the slope of the yield surface in the shear-pressure plane which was set to 11.45°, representative of a typical yield surface in a pressure dependent polymer (see Fig. 2 (c-d)). Detailed finite element simulations of the layer compression test and conditions under which it approximates a uniform state of uniaxial strain have been previously reported[20].

Fig. 1 (a) shows a stress-strain curve of uniaxial strain compression of the simulated pressure dependent polymer material which was described above. Comparing this to uniaxial strain for a non-pressure dependant (or "linear") polymer reveals key differences and similarities. In both cases we observe two distinct loading regimes (elastic and plastic) separated by a yield transition defined by a

sudden slope change or 'kink', but including pressure dependency introduces notable differences. Firstly and most prominently, is the increase in the value of stress at the yield kink, with the pressure dependent polymer exhibiting a yield transition 44% higher than would be the case for an identical linear material. This is expected from a the pressure dependent yield surface discussed above, necessitating a higher yield point as defined by the slope of the yield surface. Fig. 1 (b) shows a shear-pressure plot of the simulated material throughout the indent, showing clearly the increasing yield surface as pressure is applied. The shear increases rapidly throughout elastic loading, up until it reaches a critical value (yield), at which point the material can sustain no more shear and deforms plastically, the magnitude of shear in the material maintaining a value equivalent to the yield surface.

The second difference of note is the nonlinearity in both the purely elastic and subsequent elastic-plastic region of loading. In the standard US case, both of these regions are linear with slopes corresponding to the confined modulus *M* (in the elastic region), and bulk modulus *K* (in the plastic region), where *M* and *K* are as follows:

$$M = \frac{E(1-\nu)}{(1+\nu)(1-2\nu)} \tag{4}$$

$$K = \frac{E}{3(1-2\nu)} \tag{5}$$

Where ν is the Poisson's ratio of the material and E is the Young's modulus. However in the pressure dependent case, there is a clear upward curvature present in both regimes, caused by an increasing elastic modulus as the pressure increases and free volume is removed.

There exists in the unloading portion of the stress-strain curve a kink similar to that observed at the yield point during loading. This may be attributed to the generation of shear stress as the material relaxes post-compression, resulting in another intersection with the yield surface. This is a result of the confining well stress imposed on the material as it recovers while the uniaxial pressure is eased. Fig.1 (b) shows the decreasing shear stress on the material as we unload. The forces governing the

shear stress within the material reduce to zero, then grow in the opposite direction as the material recovers in its confined geometry. This results in a second intersection with the yield surface as the shear can increase no further within the material, and a second distinguishable kink in the unloading portion of the stress-strain curve.

Pressure Dependent Stiffness of Polystyrene Thin Film

These pressure effects have been observed in uniaxial strain measurements on bulk materials ranging from amorphous materials like polymers[16] to granular soil systems[17, 19] and metallic composites[18] . However it has been unclear whether such effects would manifest in the same way for the range of emerging thin film materials, for which there has been no ubiquitous means of uniaxial strain testing. Through our LCT measurements on thin film PS and a granular graphene network we examine the extent to which we observe these effects in the case of these thin film amorphous materials, and establish the LCT as a means of explorations of these effects on the family of thin film materials at large.

Fig.2 (a-b) shows LCT indents on a 191nm thick film of PS supported on a Si substrate, prepared via spin coating. A punch with a diameter of 2μm (for a contact aspect ratio of ~10:1) was used to perform the indents. Indents were performed with a constant loading rate of 0.67 mN/s (0.2 GPa/s). The resulting stress-strain curve shows features typical of US, including two regions of approximately linear loading (elastic followed by plastic) separated by a clear kink at the change of slope denoting the confined yield point. There exists an inflection in the curve around 0.16 strain, denoting a confinement failure of the surrounding film jacket. At this point the lateral stress overcomes the stiffness of the film jacket, and the compressed puck of material 'extrudes' outwards into the surrounding film[21]. Finally, there exists a region of slight curvature around zero strain, a result of residual misalignment of the tip to the sample surface. This results in an increasing stiffness as the punch gradually comes into full contact with the surface, and is a geometric effect not associated with the stiffness increase caused

by pressure effects. The point where the punch comes into full contact with the film is denoted in the graph.

Simultaneously with the stress-strain curve derived from the indentation load vs. displacement curve, we measured the instantaneous small amplitude dynamic stiffness by applying a controlled nanometric amplitude oscillation to the tip motion (denoted as the harmonic stiffness). This oscillation is maintained at 45Hz and an amplitude of 1nm via feedback to a force to maintain this amplitude used to determine a continuous stiffness measurement throughout the indents. The resulting harmonic stiffness vs strain graph is shown alongside the stress-strain curve in Fig.2 (a-b). While the stress-strain curvature associated with pressure dependent confined modulus is clearly defined in the FEA simulations, it is instructive for the experimental case to refer to the harmonic stiffness alongside the stress-strain response for increased clarity. While we can dismiss the increasing stiffness around zero strain resulting from incomplete punch contact, beyond this there exists a clear increase in the contact stiffness. From onset of full punch contact to the yield strain there is a ~45% increase in the harmonic stiffness from 97kN/m to 140kN/m. The corresponding curvature change in the stress-strain curve expected from such an effect is also present. This is in contrast to a non-pressure-dependant response, whereby the harmonic contact stiffness plateaus to a constant value after the region of initial punch misalignment.

Beyond the yield point into the region of plastic deformation, the harmonic stiffness continues to increase due to the pressure dependency and continued densification, the stiffness plateauing only during the onset of material extrusion (wherein the material is no longer being noticeably compressed, and instead applied stress is inducing large scale plastic flow). This clear increase in stiffness demonstrates a change of the material response with compression, attributed to collapse of free volume and densification of the material as it is compressed. While demonstrated here on PS, such effects are expected to manifest in a range of amorphous films with large degrees of free volume. Similarities between this polymer case and a similar compression on a granular nanosheet system is

presented in a later section. This demonstration of pressure dependency in LCT indents on thin film PS show clearly the presence of such effects on amorphous films and calls into question the degree to which such affects can manifest in the LCT compared to pure US compression. Yield experiments on thin film PMMA are presented to explore this.

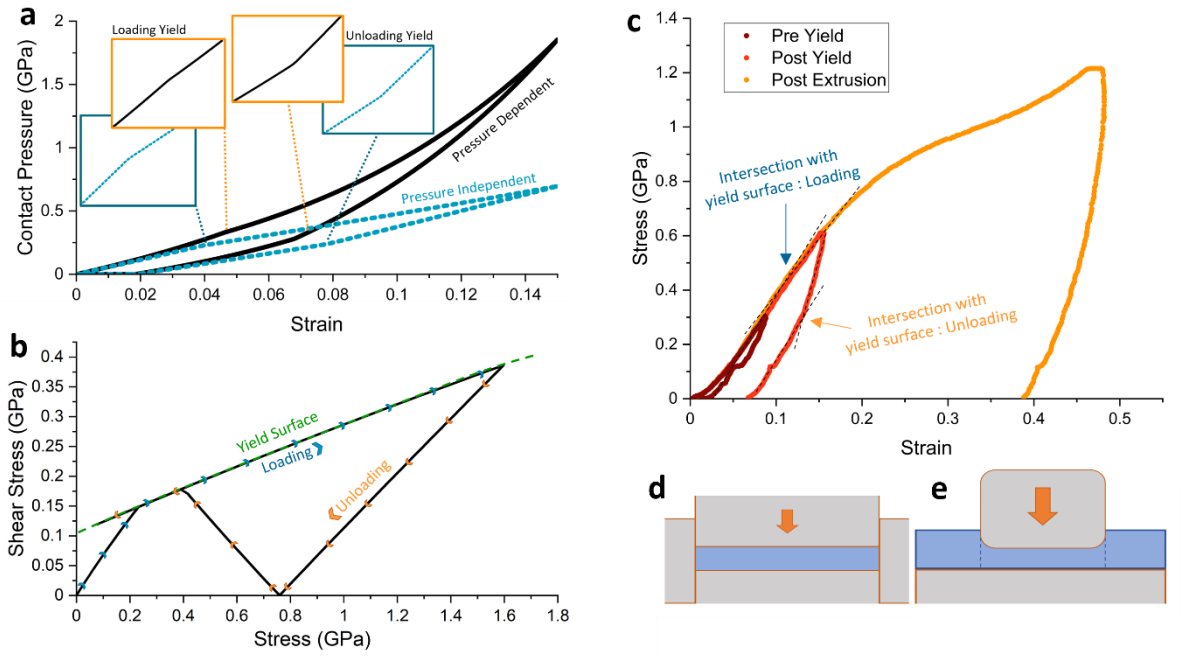

Fig.1, (a) *FEA simulated stress-strain curve (applied punch stress) of a rigidly supported polymer film under uniaxial strain compression, showing the change in modulus (curvature), as well as yield point on loading and unloading.* ***(b)*** *Shear vs compressive hydrostatic stress during the same FEA simulation, revealing the intersection with the yield surface at ~0.2 GPa on loading, and second intersection at ~0.4 GPa on unloading caused by the wall confinement.* ***(c)*** *LCT indentation of a 270nm thick PMMA film on Si substrate, with a 2µm punch (contact aspect ratio 7.4:1) showing three load-unload curves for pre-yield max stress, post-yield max stress, and post-extrusion max stress. Confined yield kink associated with intersection of the yield surface (as in* ***(b)****) is evident on the latter two, while the second intersection upon unloading is present for the post-yield indent, but not for the post-extrusion indent where US approximation has broken down.* ***(a)*** *Schematic showing uniaxial strain of a material sample,*

as used for FEA simulations, compared to ***(b)*** *LCT compression test approximating uniaxial strain condition.* ***(d-e)*** *Show schematic representation of true US and the LCT flat punch approximation, respectively*

Pressure Dependant Yield : Uniaxial Strain and the Layer Compression Test

It is interesting to note that the yield surface for some amorphous materials may increase under confined compressive stress faster than the generation of shear within the material, in principle precluding the system from ever reaching yield. In this case the material may never fail plastically due to the preponderance of hydrostatic pressure generation over shear in uniaxial strain experiments. This can be seen in Ravi-Chandar's work whereby a sample of PMMA could not be yielded in a uniaxial strain geometry[13]. This is a problem for materials testing due to the range of valuable information extractable from such US measurements. While the LCT well approximates the US condition, LCT indents on a thin film PMMA sample show a clear kink at ~0.1 strain, indicative of uniform yielding behaviour[20, 21] (270nm thick film, 2µm punch, Si substrate, 0.2 GPa/s loading rate). This is supported by the elastic response of indents with a maximum load below this kink, the plastic response of indents performed to loads higher than the kink, and the second kink present upon unloading which is expected for US compression.

In order to reconcile the existence of a yield transition in the LCT compressions of PMMA, we consider the effect of introducing excess shear into a compressed material on the yield stress. The dotted orange and yellow lines in Fig.2 (c) demonstrate how pressure dependencies can increase the yield surface in such a way that greater shear stress is needed to induce a yielding event[22] as per Eqt. (3), compared to the case of zero pressure dependency (plotted with a horizontal dashed line). The solid blue line represents the evolution of octahedral shear stress with applied pressure in a uniaxial strain geometry, and the dashed yellow line represents the case of $\mu > \frac{2\sqrt{2}}{3}\frac{G}{K}$ where the yield surface outpaces the generation of shear in US as per Eqt. (2). This demonstrates that for a material with high

enough pressure dependency yielding may be delayed indefinitely in compressive loading. In materials with such highly pressure dependant yield surfaces, uniaxial tension has been shown to introduce yielding more readily than uniaxial compression. This has been explored in bulk high contact aspect ratio experiments and pressure dependant analysis by Caruthers et al.[8, 25]. Fig. 2 (c) allows this to be visualised by the intersection of the yield surface in the tensile direction (negative pressure values), whereby the pressure dependency facilitates intersection with the yield surface at lower pressures than for compressive loading. Caruther's noted that for confined uniaxial compression, intersection with the yield surface may not be plausible for certain polymer glass systems[8]. However, introducing excess shear (effect shown by the shaded spread accompanying the solid line in Fig. 2 (c)) can increase the generation of octahedral shear stress enough to allow the exploration of material yield in otherwise difficult to yield materials while maintaining a largely uniaxial strain state.[20, 21]

For the case of PMMA, a similar increase in the shear surface slope can allow for intersection with the yield surface where normally the increase in the yield surface with applied pressure would outpace the generation of shear, as PMMA has a Von Mises pressure coefficient μ_{vm} of 0.23[26]. Taking a pressure dependent *G* and *K* into consideration explains Ravi-Chandar's result of being unable to yield PMMA in a uniaxial strain geometry, as shown in Fig.2 (d)[27]. The differences in geometry between LCT indentations and a pure US case can be examined to explain the yield behaviour observed in contrast to these experiments. We attribute increased shear generation in the LCT to the observed yield behaviour in Fig. 1 (c), which may allow exploration of yield in a closely approximated US system where one may not exist in a pure US configuration.

The most influential of these differences are the rounded punch corners, from which lateral strains propagate throughout the compressed puck[20], a non-perfectly stiff confining substrate (substrate : film stiffness ratios typically in the range of 20 for polymers on eg Si, though can be brought above 100 with stiffer substrates such as Sapphire), and elastic confining walls. This introduces more highly sheared regions in the compressed puck of material, and greater overall propagation of shear

throughout the compressed puck. This increases the slope of the shear – stress surface, and allows the material to approach the yield surface quicker, as demonstrated analytically in Fig.2 (c).

Finite element simulations of the LCT reveal the excess generation of shear stress that facilitates this effect in LCT indentations. Previous work has demonstrated the propagation of lateral stresses from the rounded punch corners during indentation[20]. This generation of lateral stresses has been shown to be greater for lower contact aspect ratios, and for lower substrate stiffnesses. This introduces regions of compressed material near the punch corners that are not under pure uniaxial compression from which shear strains can propagate. While this introduction of shear can facilitate yielding at lower stresses through altering the shear surface as discussed above, the bulk response of the compressed puck remains uniform and experiences a uniform yielding event as in uniaxial strain[20, 21].

Demonstrating this shear generation, Fig.2 (e) shows shear stress vs applied pressure in a FEA LCT compared to the case of uniaxial strain for a simulated elastic simple plastic material. Two cases are shown for clarity, one with a high aspect ratio (α) and substrate to film modulus ratio (S) (100 and 1000 respectfully) representing the more idealised case, and a lower bound of $\alpha = S = 10$, representing conditions further from US. As can be seen, the case of higher α and S limit the generation of shear stress and more closely resembles the case of US, while lowering the contact aspect ratio combined with the substrate stiffness takes us further from this case and facilitates the generation of shear stress more readily. With this effect in mind it can be important to consider the extent of shear stress generation in a confined flat punch geometry such as the LCT when considering comparisons to uniaxial strain. It can also offer useful insights into the processes controlled by introducing shear into an otherwise largely uniaxial compression and how this might affect and allow exploration of the mechanics of thin film materials (such as during a yield transition). As such the LCT can be considered an effective and tailorable tool for the exploration of pressure dependant yielding in approximated uniaxial strain compressions, allowing for controllable generation of shear and observation of yield using single dimension indentation on thin film materials.

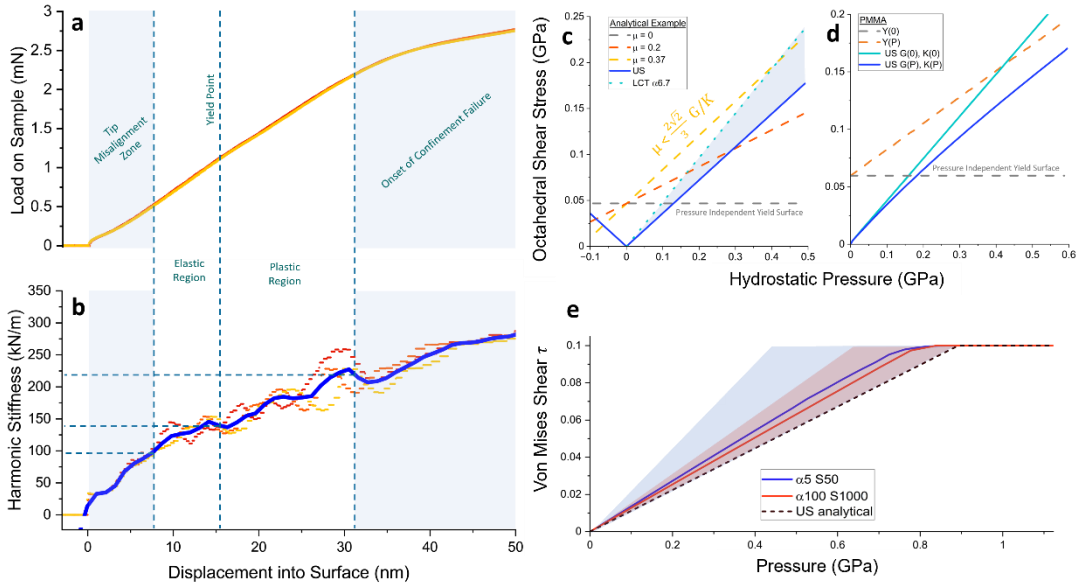

Fig.2, (a-b) *Load-displacement and continual harmonic contact stiffness data of an LCT indent on a 191nm PS indent on a Si substrate with 2µm diameter punch. Between the region of full contact and plastic yield, we observe a 45% increase in the stiffness, as well as an upwards curvature in the elastic regime of deformation, both indicative of the Modulus of the material being altered by applied pressure. The dark blue line in* ***(b)*** *represents an averaging of the three curves presented for clarity.* ***(c)*** *Octahedral shear stress vs applied pressure for a demonstrative system, detailing the increasing shear needed to cause yield in a material with a pressure sensitive yield surface as the yield surface increases with applied pressure. Example materials with yield surface pressure dependency* $\mu < \frac{2\sqrt{2}}{3}\frac{G}{K}$ *and* $\mu \geq \frac{2\sqrt{2}}{3}\frac{G}{K}$ *are both shown by dotted lines.* ***(d)*** *Pressure dependant yield surface and shear generation in uniaxial strain for PMMA. Taking the pressure dependency of the shear and bulk moduli G and K into consideration explains why US tests have previously failed to reach the pressure required for yielding in this material.* ***(e)*** *The accelerated generation of shear stress in a LCT indentation compared to pure US from finite element simulation of the LCT that can allow for intersection with the yield surface at lower pressure. The extreme cases of high contact aspect ratio (α) and substrate : film modulus ratio S, and low α and S are shown, with parameters between these extremes lying within these bounds. The solid lines represent the average Von Mises shear of all elements under the punch for each case,*

and the shaded regions represent the degree of deviation from this average for all puck elements (these deviatory elements are largely limited to those near the puck corners and so represent only a small number of overall elements)

Pressure Dependent Stiffness of Graphene Nanosheet Network

While glassy solids such as polymers experience pressure dependent effects as described above due to a decrease in internal free volume between entangled polymer chains, similar effects are often apparent in a range of amorphous materials including athermal granular materials. Samples of amorphous graphene nanosheet networks prepared by aerosol printing are considered here under testing using the LCT. Such networks are prepared via liquid phase exfoliation of bulk graphite, the resulting graphene flakes being size selected via centrifugation and prepared in a liquid dispersion[28-32]. These inks are spray coated onto flat substrates (here a silica glass microscope slide with a thin layer of sputtered gold ~50nm thick) to form networks of controllable thickness. Fig.3 (d-e) shows top down and cross section SEM images of the prepared network, which has a nominal thickness of 6.3 μm with a surface roughness of ~0.6 μm. The network flakes have an average length of 300nm and 8 layer thickness. Indents were performed with a 55 μm diameter punch for a contact aspect ratio of 8.7:1. Unlike atomic polymer chains that may thermally rattle in their free volume cages, these large flakes are expected to have negligible thermal motion relative to void sizes between the flakes. In general for granular materials, $k_B T$ is a negligible component that is superseded by the large potential energy of the grains which have masses much larger than components of a molecular system. As such the gravitic potential mgh is many orders of magnitude higher than $k_B T$ and thermodynamic considerations become negligible, and thermal motions are almost entirely suppressed through inelastic collisions[33, 34].

Sprayed nanosheet networks present many challenges to rigorous nanomechanical testing, with two effects in particular causing significant difficulty for the LCT. Firstly, the high surface roughness of these networks interferes with the required uniform stress field applied by the LCT and also introduces local

plastic deformation of surface roughness peaks before full punch contact. Secondly, the soft granular platelet nature of this system means it can experience both solid behaviour (in this case attributed mostly to the bending of individual flakes), and more liquid like deformation at longer timescales (as the flakes can slide and rearrange within the compressed volume)[34], this is exacerbated by surface roughness where initial deformation can be dominated by rearrangement of flakes on the rough surface, masking the bulk response of the puck.

To avoid these issues and to reduce the response of the network to a more clearly definable state, a series of irreversible pre-conditioning indents were performed on the region of interest. This was done by performing 4 iterative indents in the same location to a maximum load of 5 mN (2.1 MPa) with a constant loading rate of 0.05mN/s and a holdtime of 5s at max load (Fig.3 (c)). This evolved the network to a steady state in which uniaxial compression may be isolated without interference of surface roughness and a minimisation of granular flow. This establishes a well-defined geometry and framework for mechanical analysis while maintaining the qualitative nature of a porous flake network. It also has the added benefit of 'delaying' material extrusion until 5mN (as opposed to ~2.5mN on unpatterned film), which allows for a clearer examination of the pressure/density dependant stiffness to higher strains. While the authors acknowledge that this pre-patterning has some effect on the films mechanical properties compared to unpatterned film, careful analysis of these effects are not within the scope of this work and will be instead explored in a later publication, of interest here is clarifying the densification process and isolating the response of the network to a uniaxial compression.

Following the pre-processing, a single indentation was performed to peak load 6 mN with a loading rate of 0.06 mN/s. The simultaneously collected load vs. displacement and harmonic contact stiffness vs. displacement curves for this are shown in Fig.3 (a-b). The same procedure for Harmonic Stiffness as outlined earlier for the PS film is followed, with the exception that oscillation amplitude was increased to 2.5nm for clearer data collection on such a disordered system. Due to the pre-patterning, there is no tip misalignment zone present as there is in the case of the previous polymer tests

presented. Instead there exists a small zone proceeding zero strain where the indenter adjusts to sudden contact with the surface, manifesting as a settling time in the harmonic channel. Beyond this there exists a clear increase in the harmonic stiffness with applied pressure, increasing in a linear manner with strain from 20 kN/m up to 29 kN/m. Similar to that observed in polymers in the LCT and other elastic-plastic materials in US geometries, there is then a clear kink in the load-displacement and harmonic stiffness data, which we nominally label yield here, although the exact interpretation of this transition in this novel material and its relation to a traditional elastic to plastic yield point will be explored in a separate work. Similar to what we see for polymers, this kink demarks a second region of stiffness increase with a lower constant slope. The rise continues until the onset of material extrusion at 5mN, which is defined by the pre-patterning conditions as opposed to the fundamental confinement parameters of the material and indent geometry as discussed above.

As with the case of PS, we interpret this increasing stiffness as a signature of a pressure dependent modulus of the compressed puck. In polymer glasses, this is caused by a densification that arises through collapse of free volume existing between polymer chains that was left according to the specific preparation history of the sample. In the nanosheet network, the stiffness increase is also caused by a densification, but through collapse of much larger void space between flakes, with molecular changes only manifesting in the folds of the bending sheets and contributing little to the overall response.

We note the similarity in pre-yield stiffness increase in both PS and the graphene network despite very fundamental differences in material and morphology (~45% increase from contact to yield). This is in line with other elastic – yield relations between otherwise very different amorphous materials, such as a universal relation between the ratio between yield stress and Youngs modulus for otherwise very different amorphous materials[35]. In addition to this there is traction behind the idea that disordered solids share a mechanism of plasticity nucleation even between fundamentally different systems[35, 36]. Because of this, while this represents only two systems (a polymer glass and nanosheet network),

the similarity in the stiffness increase preceding yield may demonstrate a dependence on densification and free volume collapse fundamental to amorphous media, as opposed to the effect such densification has on more complex processes such as close molecular interaction and chain motions which are not ubiquitous between these materials.

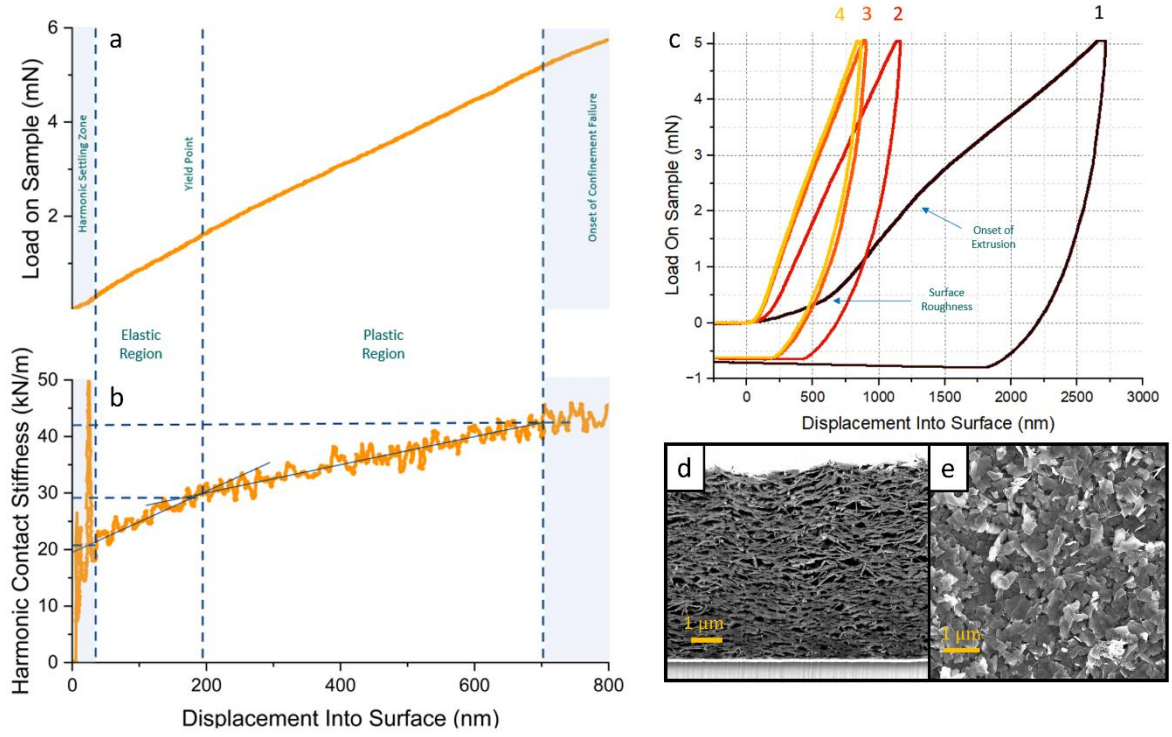

Fig.3, (a-b) *Load-displacement and continual harmonic contact stiffness data of an LCT indent on a 6.8µm thick graphene flake network on a glass substrate with a 55µm diameter punch. Flake parameters are described in the text. SEM images of a cross section performed with FIB milling is shown in* ***(d)*** *(in which the substrate and thin gold layer between can also be seen) and a top down view of the unindented, unpatterned film is shown in* ***(e)****. Beyond a settling time for the harmonic channel, stiffness of the sample increases linearly due to densification until a kink at 195nm, whereby it reduces to a new constant increase in a similar manner to polymer compression. This proceeds until confinement failure of the compressed puck at 5mN, determined by the pre patterning conditions shown in* ***(c).*** *Pre patterning consisted of 4 successive indents to 5mN in place to remove surface roughness and evolve the system to a steady state with minimal granular motion. Indent order is*

numbered and 'displacement into surface' is measured from the zero strain point of each individual indent.

Conclusion

We have presented observation and means of probing pressure dependent mechanical properties in thin films through a flat punch indentation technique dubbed the layer compression test. The uniaxial strain state approximation imposed by this technique has been compared with finite element simulations of both uniaxial strain and the LCT on pressure dependant materials and found close comparison to experiment.

Using the layer compression test, we report the observation of increasing material stiffness with densification in both elastic and plastic deformation for two amorphous thin film materials; polystyrene and an exfoliated graphene sheet network, with the results having implications for the family of amorphous free volume materials at large. We also report observed yield in thin film PMMA, a material which has previously been found not to yield under a compressive uniaxial strain condition. We attribute this to the injection of additional shear by the layer compression test, allowing for the shear generation to surpass the yield surface criteria despite a strong pressure dependency of the yield criteria in PMMA. The non-uniformity introduced by shear injection in the LCT does not mask the collective yield behaviour typical of a US yielding event. The degree of shear generation is tailorable via the contact aspect ratio and substrate stiffness and so can allow for explorations of the elastic – plastic transition in materials that are otherwise difficult to yield in such geometries.

These results can help forward the exploration of deformation and yield in thin film amorphous materials, for which sample density plays an important role but is otherwise difficult to probe and poorly understood for thin films.

References

1. Falk, M.L. and J.S. Langer, *Dynamics of viscoplastic deformation in amorphous solids.* Physical Review E, 1998. **57**(6): p. 7192-7205.
2. Falk, M.L., *Molecular-dynamics study of ductile and brittle fracture in model noncrystalline solids.* Physical Review B, 1999. **60**(10): p. 7062-7070.
3. Langer, J.S., *Shear-transformation-zone theory of deformation in metallic glasses.* Scripta Materialia, 2006. **54**(3): p. 375-379.
4. Allen, C.W. and K.C. Liao, *Dislocation Models for Shear Transformations.* physica status solidi (a), 1982. **74**(2): p. 673-681.
5. Takeuchi, S. and K. Edagawa, *Atomistic simulation and modeling of localized shear deformation in metallic glasses.* Progress in Materials Science, 2011. **56**(6): p. 785-816.
6. R. O. Davis, A.P.S.S., *Plasticity and Geomechanics*. 2001: Cambridge University Press.
7. Kazimi, S.M.A., *Solid Mechanics*. 2001: Tata McGraw-Hill.
8. Kim, J.W., G.A. Medvedev, and J.M. Caruthers, *Observation of yield in triaxial deformation of glassy polymers.* Polymer, 2013. **54**(11): p. 2821-2833.
9. Roth, C.B., *Polymer Glasses*. 1 ed. 2016, Boca Raton: CRC Press. 572.
10. Ward, I.M., *Review: The yield behaviour of polymers.* Journal of Materials Science, 1971. **6**(11): p. 1397-1417.
11. Roscoe, K.H. and J. Burland, *On the generalized stress-strain behaviour of wet clay.* 1968.
12. Roscoe, K., A. Schofield, and A. Thurairajah, *Yielding of clays in states wetter than critical.* Geotechnique, 1963. **13**(3): p. 211-240.
13. Ravi-Chandar, K. and Z. Ma, *Inelastic deformation in polymers under multiaxial compression.* Mechanics of Time-Dependent Materials, 2000. **4**: p. 333-357.
14. Roland, C., et al., *Supercooled dynamics of glass-forming liquids and polymers under hydrostatic pressure.* Reports on Progress in Physics, 2005. **68**(6): p. 1405.
15. Fujimoto, D., et al. *8Li Spin Relaxation as a Probe of the Modification of Molecular Dynamics by Inelastic Deformation of Glassy Polystyrene*. in *Journal of Physics: Conference Series*. 2023. IOP Publishing.
16. Jones Parry, E. and D. Tabor, *Pressure dependence of the shear modulus of various polymers.* Journal of Materials science, 1974. **9**: p. 289-292.
17. Liao, C.L., et al., *Pressure‐dependent elastic moduli of granular assemblies.* International Journal for Numerical and Analytical Methods in Geomechanics, 2000. **24**(3): p. 265-279.
18. Mehl, M.J., *Pressure dependence of the elastic moduli in aluminum-rich Al-Li compounds.* Physical Review B, 1993. **47**(5): p. 2493.
19. Assimaki, D. and E. Kausel, *An equivalent linear algorithm with frequency-and pressure-dependent moduli and damping for the seismic analysis of deep sites.* Soil Dynamics and Earthquake Engineering, 2002. **22**(9-12): p. 959-965.
20. Sinnott, A.D., O. Brazil, and G.L. Cross, *The effect of contact aspect ratio and film to substrate elastic modulus ratio on stress vs. strain up to the point of yield during flat punch thin film indentation of an elastic-plastic film.* Frontiers in Materials, 2022. **9**: p. 906204.
21. Brazil, O., et al., *In situ measurement of bulk modulus and yield response of glassy thin films via confined layer compression.* Journal of Materials Research, 2020. **35**(6): p. 644-653.
22. Hughes, D.S. and J.L. Kelly, *Second-Order Elastic Deformation of Solids.* Physical Review, 1953. **92**(5): p. 1145-1149.
23. Crook, A.J.L., et al., *Predictive modelling of structure evolution in sandbox experiments.* Journal of Structural Geology, 2006. **28**(5): p. 729-744.
24. Bigoni, D. and A. Piccolroaz, *Yield criteria for quasibrittle and frictional materials.* International Journal of Solids and Structures, 2004. **41**(11): p. 2855-2878.
25. Kim, J.W., G.A. Medvedev, and J.M. Caruthers, *Mobility evolution during tri-axial deformation of a glassy polymer.* Polymer, 2014. **55**(6): p. 1570-1573.

26. Quinson, R., et al., *Yield criteria for amorphous glassy polymers.* Journal of Materials Science, 1997. **32**(5): p. 1371-1379.
27. Stephens, D., H. Heard, and R. Schock, *High-pressure mechanical properties of polymethylmethacrylate*. 1972, California Univ., Livermore (USA). Lawrence Livermore Lab.
28. Backes, C., et al., *Guidelines for Exfoliation, Characterization and Processing of Layered Materials Produced by Liquid Exfoliation.* Chemistry of Materials, 2017. **29**(1): p. 243-255.
29. Kelly, A.G., et al., *All-printed thin-film transistors from networks of liquid-exfoliated nanosheets.* Science, 2017. **356**(6333): p. 69.
30. Hernandez, Y., et al., *High-yield production of graphene by liquid-phase exfoliation of graphite.* Nature Nanotechnology, 2008. **3**(9): p. 563-568.
31. Paton, K.R., et al., *Scalable production of large quantities of defect-free few-layer graphene by shear exfoliation in liquids.* Nature Materials, 2014. **13**(6): p. 624-630.
32. Coleman, J.N., *Liquid Exfoliation of Defect-Free Graphene.* Accounts of Chemical Research, 2013. **46**(1): p. 14-22.
33. Lun, C.K.K., et al., *Kinetic theories for granular flow: inelastic particles in Couette flow and slightly inelastic particles in a general flowfield.* Journal of Fluid Mechanics, 1984. **140**: p. 223-256.
34. Jaeger, H.M., S.R. Nagel, and R.P. Behringer, *Granular solids, liquids, and gases.* Reviews of Modern Physics, 1996. **68**(4): p. 1259-1273.
35. Cubuk, E.D., et al., *Structure-property relationships from universal signatures of plasticity in disordered solids.* Science, 2017. **358**(6366): p. 1033-1037.
36. Argon, A.S., *The Physics of Deformation and Fracture of Polymers.* MRS Bulletin, 2014. **39**(8): p. 747-747.